

OPTIMAL BACTERIAL RESOURCE ALLOCATION STRATEGIES IN BATCH PROCESSING*

AGUSTÍN GABRIEL YABO[†], JEAN-BAPTISTE CAILLAU[‡], AND JEAN-LUC GOUZÉ[§]

Abstract. The study of living microorganisms using resource allocation models has been key in elucidating natural behaviors of bacteria, by allowing allocation of microbial resources to be represented through optimal control strategies. The approach can also be applied to research in microbial cell factories, to investigate the optimal production of value-added compounds regulated by an external control. The latter is the subject of this paper, in which we study batch bioprocessing from a resource allocation perspective. Based on previous works, we propose a simple bacterial growth model accounting for the dynamics of the bioreactor and intracellular composition, and we analyze its asymptotic behavior and stability. Using optimization and optimal control theory, we study the production of biomass and metabolites of interest for infinite- and finite-time horizons. The resulting optimal control problems are studied using Pontryagin’s Maximum Principle and numerical methods, and the solutions found are characterized by the presence of Fuller phenomenon (producing an infinite set of switching points occurring in a finite-time window) at the junctions with a second-order singular arc. The approach, inspired in biotechnological engineering, aims to shed light upon the role of cellular composition and resource allocation during batch processing and, at the same time, poses very interesting and challenging mathematical problems.

Key words. mathematical systems theory; nonlinear systems; mathematical cell model dynamics and control; industrial biotechnology; optimal control; bacterial resource allocation

MSC codes. 37N25, 49K15, 92C42

1. Introduction. The study of living microorganisms through resource allocation models has become increasingly relevant for its capacity to elucidate natural behaviors of microbia through very simple dynamical models [7, 9, 12, 13, 21, 25]. The core idea is to represent the distribution of cellular resources through optimal control strategies, based on the assumption that evolutionary processes have tuned these endogenous allocation strategies to attain nearly-optimal levels [14]. Numerous problems arise in this context, one of them being the optimal production of metabolites regulated by an external control capable of arresting bacterial growth [11]. Growth control has proven a key engineering method for several industrial applications, such as in food preservation, biofuel production, and in combating antibiotics resistance [10]. To this end, a resource allocation approach can help understand how to modify the naturally-evolved allocation strategies so as to efficiently produce such chemical compounds [6].

These biosynthetic strategies have been studied in different frameworks. The simplest case describes the interactions between intracellular proteins with minimal interplay with the environment [27, 5, 22]. The latter can be modelled by omitting the dynamics of the substrate in the medium, representing the case where bacterial exponential growth can be attained. Another relevant, more complex case is continuous bioreactors [23, 26], used extensively in industries and in cell biology research for its capacity to reach and maintain steady-state growth conditions. The latter is

*Submitted to the editors 30th June 2022.

Funding: This work was partially supported by ANR project Maximic (ANR-17-CE40-0024-01), Ctrl-AB (ANR-20-CE45-0014), Inria IPL Cosy and Labex SIGNALIFE (ANR-11-LABX-0028-01).

[†]MISTEA, Université Montpellier, INRAE, Institut Agro, Montpellier, France (agustin.yabo@inrae.fr, www.agustinyabo.com.ar)

[‡]Université Côte d’Azur, CNRS, Inria, LJAD, France (jean-baptiste.caillau@univ-cotedazur.fr)

[§]Université Côte d’Azur, Inria, INRAE, CNRS, Sorbonne Université, Macbes Team, Sophia Antipolis, France (jean-luc.gouze@inria.fr)

42 accomplished through an inflow of fresh medium rich in substrate and an outflow of
43 the culture at the same volumetric flow rate, which produce a constant volume of the
44 culture in the device. In that case, optimization studies are mostly oriented to reach
45 such steady state in a cost-effective way. In fed-batch fermentation, the process starts
46 with an initial volume of bacterial culture inside a bioreactor, which is progressively
47 filled up through an inflow of rich medium, increasing the volume of the culture until
48 it reaches a maximum level [24]. Once the maximum volume is attained, the culture
49 evolves as a closed process, known in the field as batch processing. As no mass comes
50 in or out of the device, the remainder of the nutrients in the medium are progressively
51 consumed until the mass is entirely transformed into final products.

52 The latter is the subject of this paper, which tackles batch processing from a
53 resource allocation perspective. The novelty of the approach lies in the nature of the
54 model that—in addition to the physical and chemical laws found in classical biore-
55 actor models—considers cellular composition, taking into account the intracellular
56 components responsible for the main biological functions of bacteria. The problem
57 has been first posed in [27], where a simpler mathematical model of resource alloca-
58 tion is studied through numerical optimal control. The study does not consider the
59 dynamical aspects of the model, neither the theoretical specifics arising from the opti-
60 mal control problem and its singular arcs. We extend these results from an analytical
61 perspective—both for the dynamical analysis and the optimal control study—and in-
62 cluding the case with no metabolite synthesis as a starting point, which has not been
63 analyzed in previous works. Based on simpler bacterial growth models [7, 25] that
64 do not consider the dynamics of the substrate in the medium, a coarse-grained self-
65 replicator model is introduced, including a heterologous pathway for the production of
66 a value-added chemical compound [27, 22]. Additionally, the main biological assump-
67 tions of the mechanistic bacterial model are revised, based on empirical studies of
68 exponentially growing *E. coli* cultures [16]. Specifically, we consider a class of growth
69 rate-independent proteins in the cellular composition that accounts for housekeeping
70 proteins and non-active ribosomes, known to take up more than 50% of the cell [17].
71 The inclusion of this class of proteins in previous models has shown considerable im-
72 provement in the agreement between simulations and experimental data [25]. Using
73 mass conservation laws related to the closeness of the bioprocess, it is possible to
74 analyze the asymptotic behavior and stability of the dynamical system, showing that,
75 for every possible allocation strategy, all component of the system are transformed
76 either into proteins or into metabolites, a condition later defined as *Full depletion*.
77 Then, two main studies are performed: the biomass maximization case, representing
78 the natural objective of wild-type (i.e not modified) microbial cultures; and the me-
79 tabolite maximization case, using the full bacterial model that includes the pathway
80 for metabolite synthesis for industrial purposes. Both problems are analyzed in infi-
81 nite time and in finite time, the latter stated as OCPs (Optimal Control Problems),
82 which are investigated through the application of PMP (Pontryagin’s Maximum Prin-
83 ciple) [15]. While the finite-time case is suitable for representing bioprocesses with
84 predetermined duration, the analysis of the infinite-time case becomes crucial in un-
85 derstanding the nature and asymptotic trend of the process. The solutions of the
86 OCPs are characterized by the presence of Fuller’s phenomenon [3], producing arcs
87 composed of an infinite set of switching points (*i.e.* bangs) over a finite-time window.
88 These optimal solutions follow a Fuller-singular-Fuller structure, similar to the one
89 found in [25], described by a single second-order singular arc which is delimited by
90 two Fuller’s arcs at the beginning and at the end of the process. In particular, the
91 solution of the biomass maximization case is thoroughly studied from an analytical

92 point of view, resulting in an explicit expression of the singular control in feedback
 93 form. The results here presented are also confirmed by simulations obtained with
 94 Bocop [18], an optimal control solver based on direct methods, and published in the
 95 ct gallery¹ in order to guarantee the reproducibility of the numerical results.

96 The paper is organized as follows: in Section 2, the dynamical model is pre-
 97 sented, and its dynamical behavior is studied in Section 3. The biomass and product
 98 maximization cases are introduced and investigated in Sections 4 and 5, respectively.
 99 Finally, the results are discussed in Section 6.

100 2. Model definition.

101 **2.1. Self-replicator model.** We define a self-replicator model describing the
 102 dynamics of a microbial population growing inside a closed bioreactor. The bacterial
 103 culture has constant volume \mathcal{V}_e , measured in liters. At the beginning of the experience,
 104 there is an initial mass of substrate S inside the bioreactor, that is gradually consumed
 105 by the bacterial population, and transformed into precursor metabolites P. These
 106 precursors are intermediate metabolites used to produce proteins—such as ribosomes
 107 and enzymes—responsible for specific cellular functions; and metabolites of interest
 108 X which are excreted from the cell. The proteins forming bacterial cells are divided
 109 into three classes M, R and Q, associated to the following cellular functions:

110 **Class M** Proteins of the metabolic machinery, responsible for the uptake of nutri-
 111 ents S from the medium, the production of precursor metabolites P, and the
 112 synthesis of metabolites of interest X.

113 **Class R** Proteins of the gene expression machinery (such as ribosomes) actively in-
 114 volved in protein biosynthesis (*i.e.* in the production of proteins of classes M,
 115 Q and R).

116 **Class Q** Growth rate-independent proteins, such as housekeeping proteins respon-
 117 sible for cell maintenance, and ribosomes not involved in protein synthesis
 118 [17].

119 From a biological perspective, the production of proteins M, R and Q is catalyzed by
 120 ribosomal proteins R, and the absorption of S and synthesis of X are both catalyzed
 121 by the metabolic proteins M. This catalytic effect is represented in Figure 1 through
 122 dashed arrows. Intracellular proteins are produced at a synthesis rate V_R measured
 123 in grams per hour. The synthesis rates of proteins M, R and Q are $r_{\max}(1 - u)V_R$,
 124 $r_{\max}uV_R$ and $(1 - r_{\max})V_R$, respectively; where the parameter r_{\max} is a certain em-
 125 pirical constant imposing a maximum threshold to the rate of production of proteins
 126 M and R. The proportion of precursors dedicated to the production of growth rate-
 127 independent proteins Q is fixed, while the balance between proteins M and R is
 128 decided by the allocation control u . The latter is modelled through a time-varying
 129 function $u(t) \in [0, 1]$, where $u = 0$ means no production of ribosomal proteins R, and
 130 $u = 1$ means no production of metabolic proteins M. Depending on the objective to
 131 be analyzed, the control u can represent different mechanisms. First, it can account
 132 for the natural allocation used by bacteria, as modelled in [7, 25], by assuming that
 133 the native regulatory mechanisms of bacterial cells have been tuned by the natural
 134 selection to maximize growth rate. On the other hand, it can represent the artifi-
 135 cially modified allocation modelled in [27]. In a biotechnological setting, the latter
 136 is accomplished by engineering a synthetic growth switch that allows to modify the
 137 natural allocation through external compounds like IPTG².

¹ct.gitlabpages.inria.fr/gallery/substrate/depletion.html

²Isopropyl β -D-1-thiogalactopyranoside

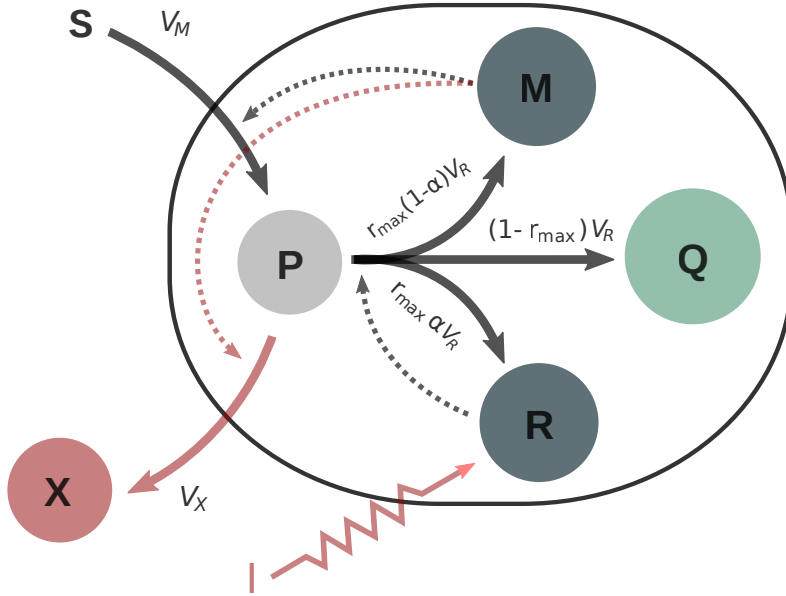


FIG. 1. *Self-replicator model of bacterial growth representing the intracellular micro-chemical reactions behind nutrient uptake, cell growth and metabolite synthesis. Solid arrows represent flow of resources resulting from the microchemical reactions, while dashed arrows indicate a catalyzing effect (i.e. the presence of a protein accelerating the synthesis of another protein).*

138 **2.2. Dynamical system.** The dynamics of the self-replicator system are de-
 139 scribed by

$$\begin{cases} \dot{S} = -V_M, \\ \dot{P} = V_M - V_X - V_R, \\ \dot{R} = r_{\max} u V_R, \\ \dot{M} = r_{\max} (1 - u) V_R, \\ \dot{Q} = (1 - r_{\max}) V_R, \\ \dot{X} = V_X, \end{cases}$$

142 where the variables $S(t)$, $P(t)$, $R(t)$, $M(t)$, $Q(t)$ and $X(t)$ represent the masses (in
 143 grams) of substrate, precursors metabolites, the gene expression machinery, the meta-
 144 bolic machinery, the growth rate-independent proteins and the metabolites of interest
 145 at time t measured in hours, respectively. $V_M(t)$, $V_R(t)$ and $V_X(t)$ are the reaction
 146 rates of the system (in grams per hour), and $u(t)$ is the allocation control previously
 147 defined. We define the volume (in liters) of the bacterial population in the bacterial
 148 culture $\mathcal{V}(t)$ as

$$(2.1) \quad \mathcal{V} \doteq \beta(M + R + Q),$$

151 where β is a constant relating protein density and volume [2]. Definition (2.1) pur-
 152 posely neglects the mass of precursor metabolites $P(t)$, which greatly simplifies the
 153 computations. The latter assumption is based on the fact that most of the mass in
 154 bacterial cells corresponds to proteins of classes M, R and Q, as confirmed in previous

155 studies [7]. This allows to define time-varying intracellular concentrations (in grams
156 per liter) with respect to this volume

$$157 \quad (2.2) \quad p \doteq \frac{P}{\mathcal{V}}, \quad r \doteq \frac{R}{\mathcal{V}}, \quad m \doteq \frac{M}{\mathcal{V}}, \quad q \doteq \frac{Q}{\mathcal{V}}.$$

159 Likewise, we define the extracellular concentrations related to the external volume

$$160 \quad (2.3) \quad s = \frac{S}{\mathcal{V}_e}, \quad x = \frac{X}{\mathcal{V}_e}.$$

162 We define the relative synthesis rates involved in the processes as increasing functions
163 of the concentrations used in each reaction [17], and taking into account the catalytic
164 effect previously described

$$165 \quad v_M(s, m) \doteq \frac{V_M}{\mathcal{V}}, \quad v_R(p, r) \doteq \frac{V_R}{\mathcal{V}}, \quad v_X(p, m) \doteq \frac{V_X}{\mathcal{V}}.$$

167 From (2.1) and (2.2), we have that

$$168 \quad (2.4) \quad m + r + q = \frac{1}{\beta},$$

170 which implies that the concentrations m , r and q cannot be bigger than $1/\beta$. We
171 define the growth rate of the bacterial culture μ as

$$172 \quad \mu \doteq \frac{\dot{\mathcal{V}}}{\mathcal{V}} = \beta v_R(p, r).$$

174 Then, the dynamical system can be expressed in terms of the concentrations as

$$175 \quad \left\{ \begin{array}{l} \dot{s} = -v_M(s, m) \frac{\mathcal{V}}{\mathcal{V}_e}, \\ \dot{p} = v_M(s, m) - v_X(p, m) - v_R(p, r)(\beta p + 1), \\ \dot{r} = (r_{\max} u - \beta r) v_R(p, r), \\ \dot{m} = (r_{\max}(1 - u) - \beta m) v_R(p, r), \\ \dot{q} = ((1 - r_{\max}) - \beta q) v_R(p, r), \\ \dot{\mathcal{V}} = \beta v_R(p, r) \mathcal{V}, \\ \dot{x} = v_X(p, m) \frac{\mathcal{V}}{\mathcal{V}_e}. \end{array} \right.$$

177 **2.3. Kinetics definition.** We model the kinetics of the system by supposing
178 that both the synthesis rates of precursors v_M and metabolites v_X are linear in the
179 concentration of metabolic proteins m , and the protein synthesis rate v_R is linear in
180 the concentration of active ribosomal proteins r [16]. Thus, they can be expressed as

$$181 \quad v_M(s, m) = w_M(s)m,$$

$$182 \quad v_R(p, r) = w_R(p)r,$$

$$183 \quad v_X(p, m) = \gamma w_R(p)m,$$

185 where $\gamma > 0$ is a proportionality constant, which allows the metabolite synthesis
 186 rate to be expressed as $v_X(p, m) = \gamma v_R(p, r) m/r$. Such assumption implies that
 187 the bacterial cell has the same affinity to synthesize biomass and metabolites from
 188 the precursors, even if the reactions do not consume P in the same proportion. In
 189 the particular case of Michaelis-Menten kinetics, this feature is captured by the half-
 190 saturation constant [8]. The functions w_I are assumed to have the following properties:

191 *Hypothesis 2.1.* Function $w_I(x) : \mathbb{R}_+ \rightarrow \mathbb{R}_+$ is

- 192 • Continuously differentiable w.r.t. x ,
- 193 • Null at the origin: $w_I(0) = 0$,
- 194 • Strictly monotonically increasing: $w'_I(x) = \frac{\partial}{\partial x} w_I(x) > 0, \forall x \geq 0$,
- 195 • Strictly concave downwards: $w''_I(x) = \frac{\partial^2}{\partial x^2} w_I(x) < 0, \forall x \geq 0$,
- 196 • Upper bounded: $\lim_{x \rightarrow \infty} w_I(x) = k_I > 0$.

197 For numerical simulations, we resort to the particular case where the functions follow
 198 Michaelis-Menten kinetics. For that case, we define

$$199 \quad w_R(p) \doteq k_R \frac{p}{K_R + p}, \quad w_X(p) \doteq k_X \frac{p}{K_X + p}, \quad w_M(s) \doteq k_M \frac{s}{K_M + s},$$

201 where the values of the constants k_R, K_R, k_X, K_X, k_M and K_M are based on the
 202 literature [7, 27]. For the general case introduced in Hypothesis 2.1, we define

$$203 \quad k_R \doteq \lim_{p \rightarrow \infty} w_R(p), \quad k_X \doteq \lim_{p \rightarrow \infty} w_X(p), \quad k_M \doteq \lim_{s \rightarrow \infty} w_M(s).$$

205 **2.4. Mass fraction formulation and non-dimensionalization.** We define
 206 non-dimensional mass fractions

$$207 \quad (2.5) \quad \hat{s} \doteq \beta s, \quad \hat{p} \doteq \beta p, \quad \hat{r} \doteq \frac{\beta}{r_{\max}} r, \quad \hat{m} \doteq \frac{\beta}{r_{\max}} m, \quad \hat{q} \doteq \beta q, \quad \hat{x} \doteq \beta x,$$

209 where \hat{r} and \hat{m} are the mass fractions of the maximal ribosomal fraction r_{\max} . Then,
 210 given that the transcription of housekeeping proteins in bacterial cells is internally
 211 auto-regulated [20], and that the mass fraction of non-translating ribosomal proteins
 212 is constant [16], we assume that the mass fraction of growth rate-independent proteins
 213 \hat{q} varies mildly compared to the remaining states, and thus we fix

$$214 \quad (2.6) \quad \hat{q} = 1 - r_{\max},$$

216 which, replacing in (2.4), yields

$$217 \quad \hat{m} + \hat{r} = 1.$$

219 The latter implies that the metabolic fraction can be expressed in terms of the ribosomal
 220 fraction as $\hat{m} = 1 - \hat{r}$, and so the dynamical equation of \hat{m} can be removed from
 221 the system. Additionally, we see that the quantity βr represents the mass fraction
 222 of translating ribosomal proteins in the cell which, using (2.4) and (2.6), has bounds
 223 $[0, r_{\max}]$. Thus, its upper bound is given by the difference between the maximal total
 224 ribosomal mass fraction and the constant non-translating ribosomal mass fraction. In
 225 the literature [25], such values are empirically fixed to 0.5 and 0.07, respectively, and
 226 so the parameter r_{\max} is here set to 0.43 for the numerical calculations. The biomass
 227 fraction of the bacterial culture is defined as

$$228 \quad (2.7) \quad \hat{v} \doteq \frac{\mathcal{V}}{\mathcal{V}_e}.$$

230 We define the non-dimensional time $\hat{t} \doteq k_R r_{\max} t$ and the non-dimensional functions

$$231 \quad \hat{w}_R(\hat{p}) = \frac{w_R(p)}{k_R}, \quad \hat{w}_X(\hat{p}) = \frac{w_X(p)}{k_R}, \quad \hat{w}_M(\hat{s}) = \frac{w_M(s)}{k_R}$$

233 so that $\lim_{\hat{p} \rightarrow \infty} \hat{w}_R(\hat{p}) = 1$. For the sake of simplicity, let us drop all hats from the
234 current notation. Thus, the system becomes

$$235 \quad (\text{S}) \quad \begin{cases} \dot{s} = -w_M(s)(1-r)\mathcal{V}, \\ \dot{p} = w_M(s)(1-r) - \gamma w_R(p)(1-r) - w_R(p)r(p+1), \\ \dot{r} = (u-r)w_R(p)r, \\ \dot{\mathcal{V}} = w_R(p)r\mathcal{V}, \\ \dot{x} = \gamma w_R(p)(1-r)\mathcal{V}. \end{cases}$$

237 In this formulation, and using (2.2), (2.3), (2.4), (2.5) and (2.7), the total mass in the
238 bioreactor can be expressed in terms of the concentrations as

$$239 \quad (2.8) \quad S + P + M + R + Q + X = \frac{\mathcal{V}_e}{\beta} (s + (p+1)\mathcal{V} + x).$$

241 3. Model analysis.

242 LEMMA 3.1. *The set*

$$243 \quad \Gamma = \{(s, p, r, \mathcal{V}, x) \in \mathbb{R}^5 : s \geq 0, p \geq 0, 1 \geq r \geq 0, \mathcal{V} \geq 0, x \geq 0\}$$

245 *is positively invariant for the initial value problem.*

246 Proving Lemma 3.1 is standard and can be done by evaluating the vector field of
247 (S) over the boundaries of Γ . Thus, we fix initial conditions

$$248 \quad (\text{IC}) \quad \begin{aligned} s(0) &= s_0 > 0, & p(0) &= p_0 > 0, & x(0) &= 0, \\ r(0) &= r_0 \in (0, 1), & \mathcal{V}(0) &= \mathcal{V}_0 > 0, \end{aligned}$$

250 where the initial concentration of metabolites $x(0)$ is set to 0 to represent the fact
251 that, at the beginning of the bioprocess, no metabolite has been produced. Some
252 relations are immediate from the dynamics: as $\dot{s} \leq 0$ and $\dot{\mathcal{V}} \geq 0$ for all t , we have

$$253 \quad (3.1) \quad s(t) \leq s_0, \quad \mathcal{V}(t) \geq \mathcal{V}_0,$$

255 representing the fact that the substrate can only be consumed (and not replenished),
256 and the biomass can only grow.

257 **3.1. Total available mass.** As typically occurs in batch processes, there is
258 neither inflow nor outflow of mass in the bioreactor, which is reflected in the dynamics
259 of the system through a mass conservation law. We define the constant

$$260 \quad \Sigma \doteq s_0 + (p_0 + 1)\mathcal{V}_0,$$

representing the initial mass concentration in the system. It can be seen that the
total mass concentration

$$z \doteq s + (p+1)\mathcal{V} + x$$

262 is constant for all t (as $\dot{z} = 0$). This means that

$$263 \quad (3.2) \quad s + (p + 1)\mathcal{V} + x = \Sigma,$$

265 for all t . Thus, relation (2.8) and (3.2) show that the total mass in the system is
 266 constant and equal to $\mathcal{V}_e \Sigma / \beta$. Variables \mathcal{V} and x are maximal when the remaining
 267 variables are equal to 0, and so they are upper bounded. In particular, both $\mathcal{V}(t)$ and
 268 $x(t)$ are decreasing w.r.t. $s(t)$ and $p(t)$. As neither s nor p can be negative, we have
 269 that

$$270 \quad (3.3) \quad \mathcal{V}(t) + x(t) = \Sigma$$

272 when $s(t) = p(t) = 0$. This condition means that all the available substrate and pre-
 273 cursor metabolites have been depleted and transformed into biomass and metabolites,
 274 which is intuitively what one would expect from system (S) for t sufficiently large.
 275 Additionally, using (3.1) and (3.2), we can obtain the following result.

276 **PROPOSITION 3.2.** $\mathcal{V}(t) \in [\mathcal{V}_0, \Sigma]$, $x(t) \in [0, \Sigma - \mathcal{V}_0]$ and $p(t) \in [0, p^+]$ for all t ,
 277 with $p^+ = \Sigma / \mathcal{V}_0 - 1$.

278 **3.2. Infinite-time full depletion.** Dynamics (S) shows that, under initial condi-
 279 tions (IC), $s(t)$ and $p(t)$ can only vanish asymptotically, that is, when $t \rightarrow \infty$. The
 280 latter can be proved by seeing that the derivatives of s and p can be bounded by

$$281 \quad \dot{s} \geq -w_M(s)\Sigma, \quad \dot{p} \geq -w_R(p)p^+(p^+ + 1 + \gamma),$$

283 which means that, at worst, s and p decay exponentially (as functions $w_i(x)$ can be
 284 upper bounded by linear functions $w_i(x) \leq c_i x$), so that $s(t) = p(t) = 0$ cannot be
 285 reached in finite time. Accordingly, we define the depletion of s and p in an infinite-
 286 time horizon.

287 **DEFINITION 3.3.** *System (S) achieves Full depletion when all the substrate and*
 288 *the precursors are asymptotically depleted, i.e.*

$$289 \quad (\text{Full depletion}) \quad \lim_{t \rightarrow \infty} s(t) = \lim_{t \rightarrow \infty} p(t) = 0,$$

291 **3.3. Asymptotic behaviour.** Now, we study the system dynamics for an infi-
 292 nite time $t \rightarrow \infty$. First, the case with a constant allocation $u(t) = u^* \in (0, 1)$ for all
 293 t is analyzed, and then an extension to a general allocation function is proposed.

294 **3.3.1. Constant allocation u^* .**

295 **THEOREM 3.4.** *For any trajectory of system (S) with initial conditions (IC) and*
 296 *constant allocation $u(t) = u^*$, it follows that*

$$297 \quad (3.4) \quad (u^* - r(t))\mathcal{V}(t) = (u^* - r_0)\mathcal{V}_0.$$

Proof. Under a constant allocation $u(t) = u^*$, the dynamics of r becomes

$$\dot{r} = (u^* - r)w_R(p)r.$$

Using dynamics (S), it is possible to see that both the total mass of proteins $R = r\mathcal{V}$
 and the quantity $U = u^*\mathcal{V}$ have the same derivative

$$\dot{R} = \dot{U} = u^*w_R(p)r\mathcal{V},$$

299 which means that the difference of these two $R_u = U - R$ should be constant (as
 300 $\dot{R}_u = 0$), which yields (3.4). \square

301 **3.3.2. General allocation** $u(t)$. Due to the boundedness of \mathcal{V} stated in Lemma 3.2, \blacksquare
 302 and the relation between \mathcal{V} and r shown in (3.2), we can see that any constant control
 303 u^* yields a bounded ribosomal fraction r . We extend this notion to any function $u(t)$.

304 **LEMMA 3.5.** *For any trajectory of system (S) with initial conditions (IC) and any*
 305 *control $u(t)$, the ribosomal concentration has bounds $r(t) \in [r^-, r^+]$ for all t , with*

$$306 \quad r^- \doteq r_0 \frac{\mathcal{V}_0}{\Sigma} > 0, \quad r^+ \doteq 1 - (1 - r_0) \frac{\mathcal{V}_0}{\Sigma} < 1.$$

308 *Proof.* Let us extend system (S) by defining variables $r_{\text{low}}(t)$ and $r_{\text{up}}(t)$ with
 309 dynamics

$$310 \quad \begin{aligned} \dot{r}_{\text{low}} &= -r_{\text{low}} w_R(p) r \leq 0, & \dot{r}_{\text{up}} &= (1 - r_{\text{up}}) w_R(p) r \geq 0, \\ r_{\text{low}}(0) &= r_0, & r_{\text{up}}(0) &= r_0, \end{aligned}$$

which correspond to the dynamics of r with $u = 0$ and $u = 1$ respectively, and which satisfy

$$r_{\text{low}}(t) \leq r(t) \leq r_{\text{up}}(t)$$

for all t . The latter can be easily proved by showing that the time-varying differences

$$\Delta_{\text{low}}(t) = r(t) - r_{\text{low}}(t), \quad \Delta_{\text{up}}(t) = r_{\text{up}}(t) - r(t)$$

with dynamics

$$\dot{\Delta}_{\text{low}} = (u - \Delta_{\text{low}}) w_R(p) r, \quad \dot{\Delta}_{\text{up}} = (1 - u - \Delta_{\text{up}}) w_R(p) r$$

312 are always non-negative: they satisfy $\Delta_{\text{low}}(0) = \Delta_{\text{up}}(0) = 0$ and are repulsive or
 313 (at worst) invariant at 0. Then, based on the same principle used to obtain (3.4),
 314 we define the quantities $R_{\text{low}} = r_{\text{low}} \mathcal{V}$ and $R_{\text{up}} = (1 - r_{\text{up}}) \mathcal{V}$ which are constant (as
 315 $\dot{R}_{\text{low}} = \dot{R}_{\text{up}} = 0$), and so

$$316 \quad r_{\text{low}}(t) = r_0 \frac{\mathcal{V}_0}{\mathcal{V}(t)}, \quad r_{\text{up}}(t) = 1 - (1 - r_0) \frac{\mathcal{V}_0}{\mathcal{V}(t)},$$

318 for all t . As $\mathcal{V}_0 \leq \mathcal{V}(t) \leq \Sigma$ for all t , we have

$$319 \quad r_{\text{low}}(t) \in \left[r_0 \frac{\mathcal{V}_0}{\Sigma}, r_0 \right], \quad r_{\text{up}}(t) \in \left[r_0, 1 - (1 - r_0) \frac{\mathcal{V}_0}{\Sigma} \right]$$

321 which shows that $r^- \leq r(t) \leq r^+$ for all t . \square

322 Lemma 3.5 states that, for any control $u(t)$, the ribosomal concentration never
 323 reaches the bounds $r = 0$ and $r = 1$, and thus neither the substrate intake nor the
 324 protein synthesis is arrested. Using this fact, it can be proved that any control $u(t)$
 325 produces (*Full depletion*).

326 **THEOREM 3.6.** *Any trajectory of system (S) with initial conditions (IC) and any*
 327 *control $u(t)$ achieves (*Full depletion*) when $t \rightarrow \infty$.*

328 *Proof.* Using Lemma 3.5, it is easy to see that

$$329 \quad \dot{s} \leq -w_M(s)(1 - r^+) \mathcal{V}_0,$$

331 which means that $s(t)$ converges to 0 as $t \rightarrow \infty$. Then, this means that

$$332 \quad \dot{p} \leq -\gamma w_R(p)(1 - r^+) - w_R(p) r^-,$$

334 and so $p(t)$ also converges to 0 as $t \rightarrow \infty$. \square

335 **4. The biomass maximization case.** In this section, we write the problem of
 336 maximizing the biomass both for infinite time and finite time in terms of the alloca-
 337 tion parameter u . The latter is a mathematical representation of the naturally-evolved
 338 resource allocation strategy used by bacteria in nature. Indeed, in biology it is very of-
 339 ten assumed that bacteria during exponential growth allocate their internal resources
 340 to maximize their growth rate, thus maximizing long-term biomass production [7].
 341 For this particular problem, we assume that no metabolite is produced, as the path-
 342 way responsible for its production is artificially engineered, and thus not present in
 343 wild-type bacteria. This is simply modeled through $\gamma = 0$. The resulting Wild-Type
 344 Bacterial Model is

$$345 \quad (\text{WTB-M}) \quad \begin{cases} \dot{s} = -w_M(s)(1-r)\mathcal{V}, \\ \dot{p} = w_M(s)(1-r) - w_R(p)r(p+1), \\ \dot{r} = (u-r)w_R(p)r, \\ \dot{\mathcal{V}} = w_R(p)r\mathcal{V}, \end{cases}$$

347 4.1. Infinite-time problem.

348 **4.1.1. Problem formulation.** We first write the biomass maximization prob-
 349 lem for an infinite-time horizon, a non-realistic scenario that can provide valuable
 350 insight into the finite-time process. Indeed, in this section, we show that the max-
 351 imum attainable performance can only be achieved in infinite-time processes. The
 352 problem can be expressed as

$$353 \quad \max_{u(t)} \lim_{t \rightarrow \infty} \mathcal{V}(t).$$

354 Since $\mathcal{V} \in [\mathcal{V}_0, \Sigma]$, applying (*Full depletion*) in (3.2) yields the condition

$$356 \quad \lim_{t \rightarrow \infty} \mathcal{V}(t) = \Sigma.$$

358 meaning that, in infinite time, the biomass is maximized for every control $u(t)$. We
 359 formalize the latter in the following theorem.

360 **THEOREM 4.1.** *For any trajectory of system (WTB-M) with initial conditions*
 361 *(IC) and any control $u(t)$, the volume $\mathcal{V}(t) \rightarrow \max \mathcal{V}(t) = \Sigma$ as $t \rightarrow \infty$.*

362 As a consequence, using Theorem 3.4, we have the following result for constant
 363 allocations.

364 **COROLLARY 4.2.** *For any trajectory of system (WTB-M) with initial conditions*
 365 *(IC) and constant control $u(t) = u^*$,*

$$366 \quad \lim_{t \rightarrow \infty} r(t) = u^* - (u^* - r_0) \frac{\mathcal{V}_0}{\Sigma}$$

368 These results are illustrated by the numerical simulations shown in next section.

369 **4.1.2. Numerical simulations.** Examples of trajectories confirming the ana-
 370 lytical results are shown in Figure 2 and Figure 3, where we see that the system
 371 approaches (*Full depletion*) asymptotically in every case, thus approaching the max-
 372 imal biomass value $\mathcal{V}(t) = \Sigma$. Figure 2 shows the resulting trajectories associated to

373 the same initial conditions, when varying the allocation parameter u . On the other
 374 hand, Figure 3 illustrates the trajectories for different values of r_0 . Indeed, as Σ does
 375 not depend on the resource allocation strategy, all the available mass is transformed
 376 into biomass independently of the values of r_0 and $u(t)$.

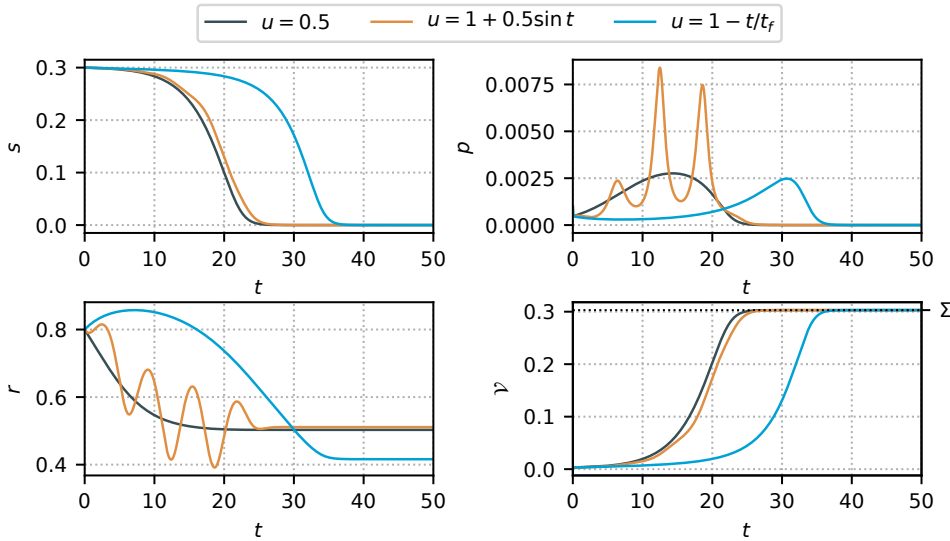


FIG. 2. Simulation of (WTB-M) with initial conditions $s_0 = 0.3$, $p_0 = 0.001$, $r_0 = 0.8$, $\mathcal{V}_0 = 0.003$, fixed final time $t_f = 50$ and different allocation functions u .

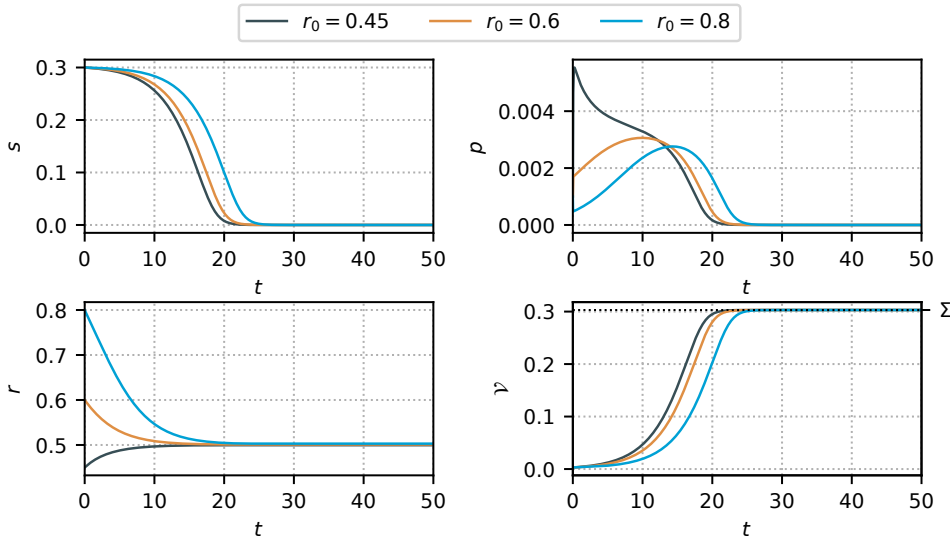


FIG. 3. Simulation of (WTB-M) with initial conditions $s_0 = 0.3$, $p_0 = 0.001$, $\mathcal{V}_0 = 0.003$, $u = 0.5$, fixed final time $t_f = 50$ and different values of r_0 .

377

4.2. Finite-time problem.

378 **4.2.1. Problem formulation.** For the Biomass Maximization problem at final
 379 time t_f , we write the OCP maximizing the final bacterial volume $\mathcal{V}(t_f)$ with initial
 380 conditions (IC):

$$381 \quad (\text{BM-OCP}) \quad \left\{ \begin{array}{l} \text{maximize} \quad \mathcal{V}(t_f), \\ \text{subject to} \quad \text{dynamics of (WTB-M)}, \\ \quad \quad \quad \text{initial conditions (IC)}, \\ \quad \quad \quad u(\cdot) \in \mathcal{U}. \end{array} \right.$$

382
 383 For this class of optimal control problem, with no terminal constraints, there are no
 384 controllability issues. Additionally, the dynamics is affine in the control, with the
 385 latter included in a compact and convex set (a closed interval), and it can be checked
 386 that every finite-time trajectory remains bounded. Thus, existence of a solution is
 387 guaranteed by Filippov's theorem [1]. Then, for a problem (BM-OCP) with state
 388 $\varphi \in \mathbb{R}^n$, PMP ensures that there exists an absolutely continuous mapping $\lambda(\cdot) : [0, t_f] \rightarrow \mathbb{R}^n$ such that the extremal (φ, λ, u) satisfies the generalized Hamiltonian system
 390 system

$$391 \quad (\text{PMP}) \quad \left\{ \begin{array}{l} \dot{\varphi} = \frac{\partial}{\partial \lambda} H(\varphi, \lambda, u), \\ \dot{\lambda} = -\frac{\partial}{\partial \varphi} H(\varphi, \lambda, u), \\ H(\varphi, \lambda, u) = \max_{u \in [0,1]} H(\varphi, \lambda, u), \end{array} \right.$$

392
 393 for almost every $t \in [0, t_f]$. We define the adjoint states for this particular case as
 394 $\lambda = (\lambda_s, \lambda_p, \lambda_r, \lambda_v)$, and we write the Hamiltonian

$$395 \quad H = -w_M(s)(1-r)\mathcal{V}\lambda_s + \left(w_M(s)(1-r) - w_R(p)r(p+1) \right) \lambda_p + w_R(p)r\mathcal{V}\lambda_v \\ 396 \quad + (u-r)w_R(p)r\lambda_r,$$

397
 398 and the adjoint system as

$$399 \quad \left\{ \begin{array}{l} \dot{\lambda}_s = w'_M(s)(1-r)(\mathcal{V}\lambda_s - \lambda_p), \\ \dot{\lambda}_p = (w'_R(p)r(p+1) + w_R(p)r)\lambda_p - w'_R(p)r\mathcal{V}\lambda_v - (u-r)w'_R(p)r\lambda_r, \\ \dot{\lambda}_r = -w_M(s)(\mathcal{V}\lambda_s - \lambda_p) + w_R(p)((p+1)\lambda_p - \mathcal{V}\lambda_v) - (u-2r)w_R(p)\lambda_r, \\ \dot{\lambda}_v = w_M(s)(1-r)\lambda_s - w_R(p)r\lambda_v. \end{array} \right.$$

400
 401 Given that there are no terminal conditions on the state, the transversality conditions
 402 for the adjoint state are $\lambda(t_f) = (0, 0, 0, 1)$. Note that $\lambda_v(t_f) = 1$ comes from the
 403 fact that the cost function is $\mathcal{V}(t_f)$ and there are no terminal conditions on the other
 404 states (this prevents the so-called *abnormal* extremals with $\lambda_v(t_f) = 0$). Since the
 405 (WTB-M) dynamics is single-input and control-affine,

$$406 \quad \dot{\varphi} = F_0(\varphi) + uF_1(\varphi)$$

407 with obvious definitions for the vector fields F_0, F_1 , the Hamiltonian writes $H =$
 408 $H_0 + uH_1$. The Hamiltonian lifts $H_i := \langle \lambda, F_i \rangle$, $i = 0, 1$, of the two vector fields are

$$\begin{aligned} 409 \quad H_0 &= -w_M(s)(1-r)\mathcal{V}\lambda_s + \left(w_M(s)(1-r) - w_R(p)r(p+1)\right)\lambda_p \\ 410 \quad &\quad + w_R(p)r\mathcal{V}\lambda_V - w_R(p)r^2\lambda_r, \\ 411 \quad H_1 &= w_R(p)r\lambda_r. \end{aligned}$$

413 The constrained optimal control u should maximize the Hamiltonian, so the solution
 414 of (BM-OCP) is

$$415 \quad (4.1) \quad u(t) = \begin{cases} 0 & \text{if } H_1 < 0, \\ 1 & \text{if } H_1 > 0, \end{cases}$$

417 while $u(t) = u_s(t)$ is called singular whenever H_1 vanishes on a whole subinterval of
 418 $[0, t_f]$. This tells that an optimal control is a (possibly very complicated) concate-
 419 nation of bangs ($u = 0$ and $u = 1$) and singular arcs, depending on the sign of the
 420 switching function H_1 . We see that, at final time, the dynamics of λ_r becomes

$$421 \quad \dot{\lambda}_r(t_f) = w_R(p(t_f))\mathcal{V}(t_f)\lambda_0 < 0,$$

423 which, using the fact that $\lambda_r(t_f) = 0$, implies that $\lambda_r > 0$ for a period $[t_f - \varepsilon, t_f]$,
 424 and thus $H_1 > 0$ for a period $[t_f - \varepsilon, t_f]$. As the control u should maximize the
 425 Hamiltonian, we have the following result.

426 **LEMMA 4.3.** *There exists ε such that the final bang arc of the optimal control*
 427 *solution of (BM-OCP) corresponds to $u(t) = 0$ for the time interval $[t_f - \varepsilon, t_f]$.*

428 A more detailed analysis of the optimal control solution can be done by studying
 429 the behavior of singular extremals. The latter is key in describing the structure of the
 430 optimal control, as it is typically associated to intermediate values of the control u
 431 (i.e. non-bang arcs). In the general case application of PMP, the singular control can
 432 be expressed as a function of the state and the adjoint state $u_s(t) = f(\varphi, \lambda)$, where the
 433 explicit expression of f can be obtained by successively differentiating the switching
 434 function H_1 until the singular control can be solved for. In the next section, we show
 435 for our problem that the singular optimal control is of order two, and that it can be
 436 expressed in feedback form as $u_s(t) = u(\varphi(t))$. In control systems design, the latter is
 437 a particular case that allows for a straightforward closed-loop implementation of the
 438 optimal control law, and that can provide further insight on the nature of the optimal
 439 trajectories.

440 **4.2.2. Singular arcs.** A singular arc occurs when H_1 vanishes (as well as its
 441 successive derivatives w.r.t. time) on a subinterval $[t_1, t_2] \subset [0, t_f]$, and so

$$442 \quad H_1 = w_R(p)r\lambda_r = 0,$$

444 As r is bounded and p cannot vanish in finite time, the condition becomes

$$445 \quad (4.2) \quad \lambda_r = 0.$$

447 We differentiate H_1 , we evaluate the expression in (4.2), and we get

$$448 \quad \dot{H}_1 = w_R(p)r \left(-w_M(s)(\mathcal{V}\lambda_s - \lambda_p) + w_R(p)((p+1)\lambda_p - \mathcal{V}\lambda_V) \right) = 0.$$

449

450 Then, the Hamiltonian can be expressed as

$$451 \quad (4.3) \quad H = -w_M(s)(\mathcal{V}\lambda_s - \lambda_p) - r\lambda_r + (u - r)H_1 = c$$

on the interval $[t_1, t_2]$, where c is a positive constant that, due to the constancy of the Hamiltonian, is equal to

$$c \doteq H(t_f) = w_R(p(t_f))r(t_f)\mathcal{V}(t_f) > 0.$$

453 Then, (4.3) implies that, over a singular arc,

$$454 \quad (4.4) \quad w_M(s)(\mathcal{V}\lambda_s - \lambda_p) = w_R(p)((p+1)\lambda_p - \mathcal{V}\lambda_{\mathcal{V}}) = -c.$$

456 Differentiating \dot{H}_1 , and evaluating over $H_1 = \dot{H}_1 = 0$, yields

$$\begin{aligned} 457 \quad \ddot{H}_1 &= w_R(p)r \left(w'_R(p)((p+1)\lambda_p - \mathcal{V}\lambda_{\mathcal{V}})(w_M(s)(1-r) - w_R(p)r(p+1)) \right. \\ 458 &\quad \left. + w_R(p)(w_M(s)(1-r) - w_R(p)r(p+1))\lambda_p \right. \\ 459 &\quad \left. + w_R(p)(p+1) \left((w'_R(p)r(p+1) + w_R(p)r)\lambda_p - w'_R(p)r\mathcal{V}\lambda_{\mathcal{V}} \right) \right. \\ 460 &\quad \left. - w_R^2(p)r\mathcal{V}\lambda_{\mathcal{V}} - w_R(p)\mathcal{V}(w_M(s)(1-r)\lambda_s - w_R(p)r\lambda_{\mathcal{V}}) \right) = 0. \\ 461 \end{aligned}$$

462 By simplifying terms and replacing with (4.4), we obtain

$$463 \quad \ddot{H}_1 = cr(1-r) \left(w_R^2(p) - w'_R(p)w_M(s) \right) = 0.$$

465 which implies that

$$466 \quad (4.5) \quad \frac{w_R^2(p)}{w_M(s)w'_R(p)} = 1. \\ 467$$

468 The fact that u does not appear in \ddot{H}_1 shows that any singular arc is at least of
469 *local order two*, so that additional derivatives should be calculated in order to retrieve
470 an explicit expression of the optimal control. Here, some precisions are in order,
471 and we may first recall that the computation can also be performed in terms of
472 Poisson brackets³ since derivating along an extremal amounts to bracketing with the
473 Hamiltonian. In particular,

$$\begin{aligned} 474 \quad \dot{H}_1 &= \{H_0 + uH_1, H_1\}, \\ 475 &= \{H_0, H_1\} =: H_{01}. \end{aligned}$$

477 Iterating, and with obvious notations ($H_{001} := \{H_0, \{H_0, H_1\}\}$, *etc.*), one obtains

$$478 \quad 0 = \dot{H}_{01} = H_{001} + uH_{101}.$$

479 (Let us recall that H_{01} is also equal to the Hamiltonian lift of the Lie bracket
480 $[F_0, F_1] =: F_{01}$, that H_{001} is the lift of $[F_0, [F_0, F_1]] =: F_{001}$, *etc.*) The previous
481 computation shows that H_{101} is zero on the subset $\{H_1 = H_{01} = 0\}$ of the cotangent
482 space. These two relations have indeed been used during the computation, while an

³In coordinates, if fg and g are two scalar valued functions of $(\varphi, \lambda) \in \mathbb{R}^{2n}$, $\{f, g\} = \sum_{i=1}^n (\partial f / \partial \lambda_i)(\partial g / \partial \varphi_i) - (\partial f / \partial \varphi_i)(\partial g / \partial \lambda_i)$.

483 explicit evaluation⁴ allows to verify that the bracket H_{101} is *not* identically zero on
 484 the whole cotangent space. In such a situation, the *local* (not *intrinsic*) order is said
 485 to be at least two; that is at least two more differentiations *wrt.* time are required to
 486 retrieve the singular control. We are actually in the following case (see also [4] for a
 487 similar analysis):

488 PROPOSITION 4.4. *If the Lie bracket F_{101} belongs to the span of F_1 and F_{01} , then*
 489 *singular extremals must be of (local) order at least two.*

490 *Proof.* By assumption, if for some φ a covector λ is orthogonal to F_1 and F_{01} at
 491 φ , it is also orthogonal to F_{101} at this point. So, along a singular extremal that must
 492 belong to $\{H_1 = H_{01} = 0\}$, one has

$$493 \quad 0 \equiv H_{001} + u_s H_{101}$$

494 with H_{101} also vanishing. As a result, $0 \equiv H_{001}$ along the singular, and one can
 495 differentiate again:

$$496 \quad 0 \equiv H_{0001} + u_s H_{1001}.$$

497 Now, by Leibniz rule

$$498 \quad H_{1001} = \{H_1, \{H_0, H_{01}\}\} = \underbrace{\{-H_{01}, H_{01}\}}_{=0} + \{H_0, H_{101}\}$$

499 and there exist smooth functions a and b of φ such that $F_{101} = aF_1 + bF_{01}$ (and
 500 similarly for the associated Hamiltonian lifts). By Leibniz rule again, H_{1001} must
 501 vanish when $H_1 = H_{01} = H_{001} = 0$ as

$$502 \quad \{H_0, aH_1 + bH_{01}\} = \{H_0, a\}H_1 + aH_{01} + \{H_0, b\}H_{01} + bH_{001},$$

503 so $H_{0001} \equiv 0$. So one has to differentiate at least once more to retrieve the control. \square

504 It should moreover be noted that \ddot{H}_1 depends only on the state—and not on the
 505 adjoint state—which implies that its successive derivatives also depend only on the
 506 state, as the adjoint state does not appear in system (WTB-M). Additionally, and
 507 based on Hypothesis (2.1), the function $w_M(s)$ is invertible, which means that s can
 508 be expressed in terms of p through equation (4.5). Once again, we differentiate \dot{H}_1 ,
 509 we evaluate over $H_1 = \dot{H}_1 = \ddot{H}_1 = 0$, and we get

$$510 \quad \begin{aligned} \dot{\dot{H}}_1 &= c(1-r)r \left(2w_R(p)w'_R(p)(w_M(s)(1-r) - w_R(p)r(p+1)) \right. \\ 511 &\quad \left. - w''_R(p)w_M(s)(w_M(s)(1-r) - w_R(p)r(p+1)) \right. \\ 512 &\quad \left. + w'_R(p)w'_M(s)w_M(s)(1-r)\mathcal{V} \right) = 0. \end{aligned}$$

514 By rearranging the expression, we can express

$$515 \quad \dot{\dot{H}}_1 = c(1-r)r(\omega_0(p, \mathcal{V}) - \omega_1(p, \mathcal{V})r) = 0,$$

⁴Take for instance $k_R = 1.1$, $k_M = 1.2$, $K_R = 1.3$, $K_M = 1.4$, $\varphi = \lambda = (1, 1, 1, 1)$ and check that $H_{101}(\varphi, \lambda) \neq 0$.

517 with

$$518 \quad \omega_0(p, \mathcal{V}) = w_M(s) \left(2w_R(p)w'_R(p) - w''_R(p)w_M(s) + w'_R(p)w'_M(s)\mathcal{V} \right) > 0,$$

$$519 \quad \omega_1(p, \mathcal{V}) = \omega_0(p, \mathcal{V}) + w_R(p)(p+1)(2w'_R(p)w_R(p) - w''_R(p)w_M(s)) > 0,$$

521 where the positivity of functions ω_i is a consequence of Hypothesis 2.1. The latter
522 shows that, along the singular arc, r can be expressed in terms of p and \mathcal{V} (as, using
523 (4.5), s can be expressed in terms of p) as

$$524 \quad r = \frac{\omega_0(p, \mathcal{V})}{\omega_1(p, \mathcal{V})}.$$

526 Then, computing the next derivative and evaluating over the obtained conditions
527 yields

$$528 \quad (4.6) \quad \ddot{H}_1 = c(1-r)r(\dot{\omega}_0(p, \mathcal{V}) - \dot{\omega}_1(p, \mathcal{V})r - \omega_1(p, \mathcal{V})(u-r)w_R(p)r) = 0.$$

530 We can see that the factor of u in expression (4.6) satisfies

$$531 \quad (4.7) \quad \frac{\partial}{\partial u} \ddot{H}_1 = -c(1-r)w_R(p)r^2\omega_1(p, s, \mathcal{V}) < 0$$

533 as $\omega_1 > 0$ for all t , which leads to the following result.

534 **THEOREM 4.5.** *The singular optimal control is exactly of order two, and it can be*
535 *expressed in feedback form, $u = u(p, \mathcal{V})$.*

536 *Proof.* Since it has been already proven that the singular arc is at least of order
537 two, it suffices to prove that it cannot be of greater order. This can be done by
538 observing that (4.7) cannot vanish. Thus, the singular arc is exactly of order two.
539 Additionally, solving for u in the same expression yields

$$540 \quad u_s(p, \mathcal{V}) = \frac{\dot{\omega}_0(p, \mathcal{V}) - \dot{\omega}_1(p, \mathcal{V})r}{\omega_1(p, \mathcal{V})w_R(p)r} + r.$$

542 which shows that the control u can be expressed as a function of the state variables.□

543 We note that the generalized Legendre-Clebsch condition, necessary for optimality of
544 the singular arc, is fulfilled in strict form by virtue of (4.7):

$$545 \quad (-1)^k \frac{\partial}{\partial u} \left(\frac{d^{2k}}{dt^{2k}} H_1 \right) = \frac{\partial}{\partial u} \ddot{H}_1 < 0.$$

547 **4.2.3. Numerical simulations.** The optimal trajectories were computed with
548 Bocop [18], which solves the OCP through a direct method. The time discretization
549 algorithm used is Lobato IIIC (implicit, 4-stage, order 6) with 2000 time steps. Figures
550 4 and 5 show optimal trajectories for the same set of initial conditions and different
551 values of t_f . Using the mass conservation law (3.2), the quantities are represented in
552 the plots as fractions of the total mass in the bioreactor $\mathcal{V}_e\Sigma/\beta$. The optimal control
553 u is characterized by the presence of chattering after and before the singular arc, as
554 expected in singular arcs of order two. From a biological point of view, both allocation
555 strategies prioritize the synthesis of proteins of the metabolic machinery M (red in
556 both Figures): the singular arc takes rather small values, and a large proportion of
557 the optimal control corresponds to a bang arc $u = 0$ at the end of the bioprocess.

558 The latter strategy promotes nutrient uptake, which results in a faster depletion of
 559 the substrate. It is interesting to note that, in opposition to previous results in the
 560 literature [7, 25], the presence of the turnpike properties [19] is not assured. Intuitively,
 561 the turnpike phenomenon would cause the time interval corresponding to the singular
 562 arc to increase as the final time t_f increases. However, a quick comparison between
 563 Figures 4 and 5 shows that this is not the case, as the increase of t_f only produces
 564 a larger 0-bang arc at the end of the bioprocess. This suggests that the duration
 565 of the initial phase dedicating a fraction of the resources to ribosomal proteins is
 566 fixed and independent of the duration of the batch process. Figure 6 also shows an
 567 optimal trajectory, but with a different initial ribosomal concentration. According
 568 to multiple simulations, this change shows an impact on the initial Fuller arc, that
 569 becomes perceptively larger, but has no major effects on the remaining of the process.
 570 Additionally, we note that the concentration of precursor metabolites in the bioreactor
 571 remains negligible in comparison with the other quantities, a result that matches the
 biological assumptions done in the modelling section.

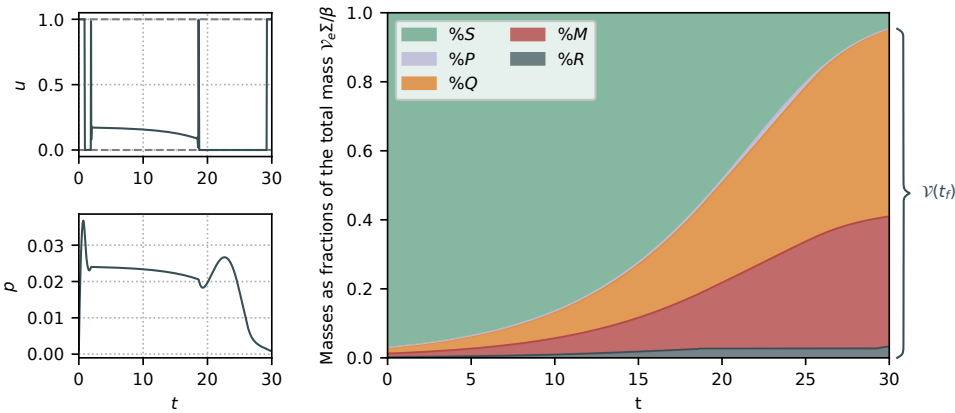


FIG. 4. Numerical simulation of (BM-OCP) with initial conditions $s_0 = 0.1$, $p_0 = 0.001$, $r_0 = 0.1$, $V_0 = 0.003$ and $t_f = 30$. Quantities in the right plot are shown as fractions of the total mass in the bioreactor $V_e \Sigma / \beta$. The final volume $V(t_f)$ is at 95% of $V_e \Sigma / \beta$.

572

573

Figure 7 illustrates optimal trajectories in the sp -plane for different final times
 574 (20, 25, 30 and 40). Each trajectory approaches the singular curve $\dot{H}_1 = 0$ given
 575 by expression (4.5) (obtained from the singular surface) through a Fuller arc, slides
 576 along it during a certain time interval, and then follows a trajectory obtained from
 577 the $u = 0$ arc that approaches asymptotically (*Full depletion*). Naturally, the longer
 578 the simulation of the process, the closer the final state to (*Full depletion*). These
 579 results also confirm the observations previously done: the duration in time of the
 580 singular arc is not directly related to the final time t_f . In fact, all the singular
 581 arcs start at approximately the same time instant and finish around $t = 18$. The
 582 independence of the initial phase from the duration of the bioprocess is coherent with
 583 the fact that bacteria allocate resources in terms of their cellular composition and the
 584 environment [7] (which, in this case, is described by the concentration of substrate in
 585 the medium), independently of the man-made notion of duration of the bioprocess. It
 586 is also noteworthy that, while the processes exit the singular surface at similar times,
 587 the trajectories differ significantly as they exit the singular arc from different initial
 588 conditions (not only in the (s, p) plane but also in the original \mathbb{R}^4 space).

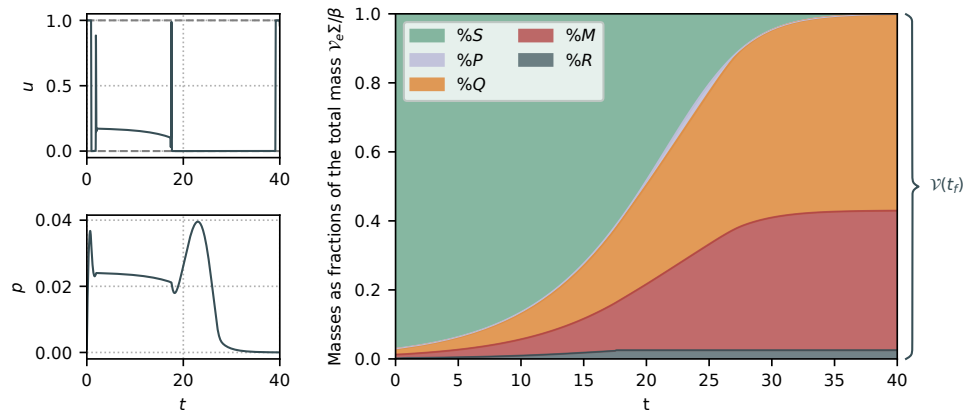


FIG. 5. Numerical simulation of (BM-OCP) with initial conditions $s_0 = 0.1$, $p_0 = 0.001$, $r_0 = 0.1$, $\mathcal{V}_0 = 0.003$ and $t_f = 40$. Quantities in the right plot are shown as fractions of the total mass in the bioreactor $\mathcal{V}_e \Sigma / \beta$. The final volume $\mathcal{V}(t_f)$ is at 99.8% of $\mathcal{V}_e \Sigma / \beta$.

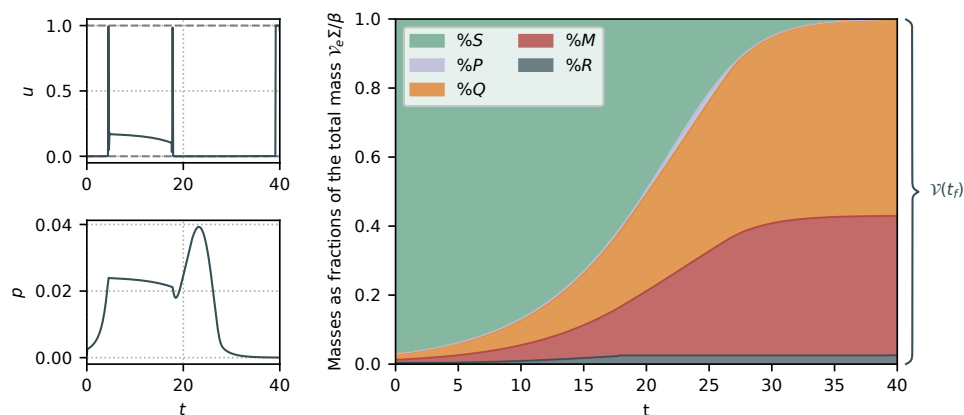


FIG. 6. Numerical simulation of (BM-OCP) with initial conditions $s_0 = 0.1$, $p_0 = 0.001$, $r_0 = 0.3$, $\mathcal{V}_0 = 0.003$ and $t_f = 40$. Quantities in the right plot are shown as fractions of the total mass in the bioreactor $\mathcal{V}_e \Sigma / \beta$. The final volume $\mathcal{V}(t_f)$ is at 99.8% of $\mathcal{V}_e \Sigma / \beta$.

4.2.4. Alternative approach: prescribed performance in minimum time. ■

589 As confirmed by the finite-time case studied in the last section, the associated opti-
 590 mal control problem with fixed final time yields a final volume $\mathcal{V}(t_f)$ that can be
 591 viewed as a fraction (between 0 and 1) of the total mass concentration in the system
 592 Σ . Indeed, Theorem 4.1 showed that \mathcal{V} can reach its maximum value Σ only when
 593 t goes to infinity. Thus, (BM-OCP) can be reformulated to achieve a minimal-time
 594 transfer between an initial state (IC) (with biomass $\mathcal{V}(0) = \mathcal{V}_0$) and a final state with
 595 terminal constraint
 596

597 (TC)

$$\mathcal{V}(t_f) = \eta \Sigma,$$

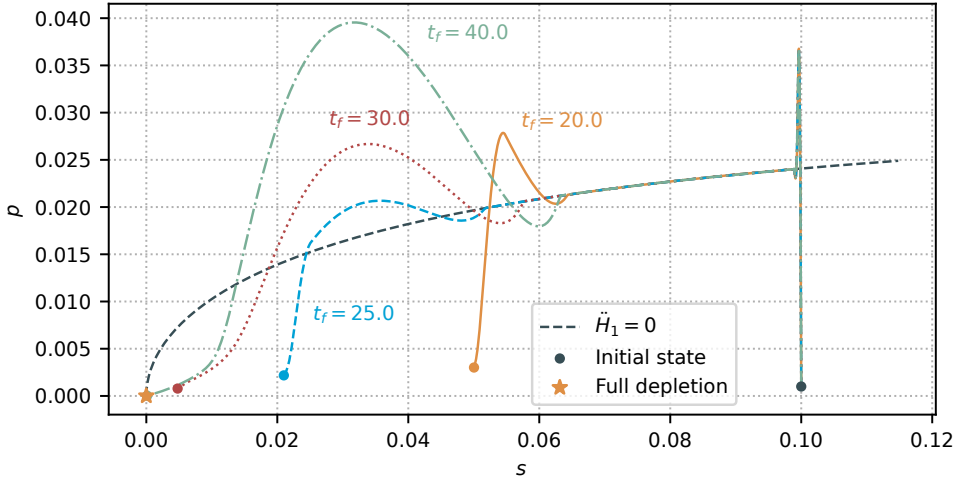


FIG. 7. Numerical simulation of (BM-OCP) showing different trajectories in the sp -plane. Initial conditions are set to $s_0 = 0.1$, $p_0 = 0.001$, $r_0 = 0.1$, $\mathcal{V}_0 = 0.003$. In all cases, the state approaches the singular curve $\dot{H}_1 = 0$ and slides along it.

599 for a certain performance parameter $\eta \in [\eta_{\min}, 1)$, where $\eta_{\min} \doteq \mathcal{V}_0/\Sigma$. The reformu-
 600 lated minimal-time OCP with Prescribed Performance writes

$$\begin{cases}
 \text{minimize} & t_f, \\
 \text{subject to} & \text{dynamics of (WTB-M),} \\
 & \text{initial conditions (IC),} \\
 & \text{terminal constraints (TC),} \\
 & u(\cdot) \in \mathcal{U}.
 \end{cases}$$

601 (PP-OCP)

602

603 A natural question arising from OCPs with terminal constraints is the existence of a
 604 solution. In this case, Theorem 4.1 guarantees that any final volume $\mathcal{V}(t_f) = \eta\Sigma$ can
 605 be reached in finite time, as long as $\eta \in [\eta_{\min}, 1)$. The latter ensures the existence of
 606 the solution for any $\eta \in [\eta_{\min}, 1)$. The study of the solutions of (PP-OCP) can
 607 be performed through an analogous PMP approach, with the difference that the
 608 Hamiltonian is null for every $t \in [0, t_f]$ due to the free final time t_f , and that there
 609 is no terminal constraint on $\lambda_{\mathcal{V}}$ (*i.e.* $\lambda_{\mathcal{V}}(t_f)$ is free). Given the similarity with the
 610 previously analyzed case, the computations of such optimal control solution are not
 611 explicated here. A numerical solution of the problem is shown in Figure 8.

612 **5. The product maximization case.** As done in the previous section, we
 613 approach the product maximization objective in infinite time and finite time using
 614 the full model (S) where $\gamma \in \mathbb{R}^+$.

615 **5.1. Infinite-time problem.** The problem of maximizing the product concen-
 616 tration at infinite time is given by the expression

$$\max_{u^*} \lim_{t \rightarrow \infty} x(t),$$

617
 618

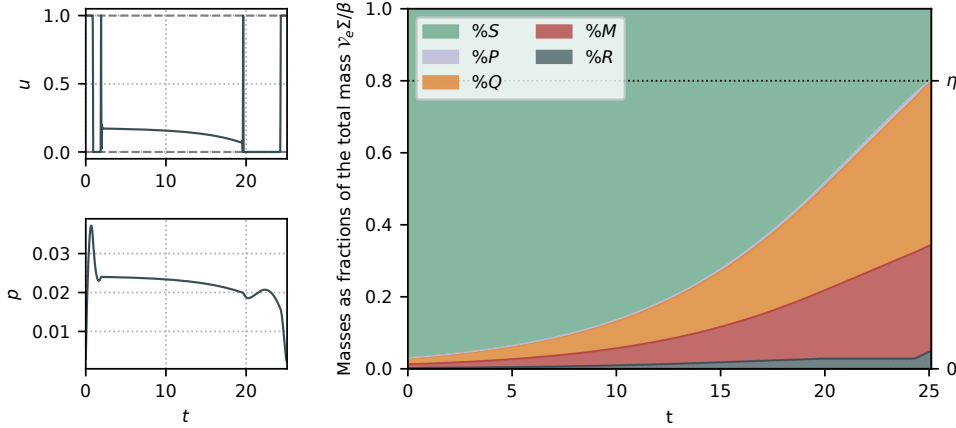


FIG. 8. Numerical simulation of (PP-OCP) with initial conditions $s_0 = 0.1$, $p_0 = 0.003$, $r_0 = 0.1$ and $\mathcal{V}_0 = 0.003$. The performance parameter is fixed to $\eta = 0.8$, which is achieved in $t_f = 25.1$. Quantities in the right plot are shown as fractions of the total mass in the bioreactor $\mathcal{V}_e \Sigma / \beta$.

619 which, using (3.3), can be rewritten as

$$620 \quad \min_{u^*} \lim_{t \rightarrow \infty} \mathcal{V}(t)$$

621
 622 indicating that maximizing the metabolite concentration at infinite time equates to
 623 minimizing the biomass. While, in the previous section, the conditions (*Full depletion*)
 624 and (3.2) were sufficient to determine the asymptotic behavior of the system, the pres-
 625 ence of x in this particular problem does not allow a similar resolution. An alternative
 626 approach, in order to better understand the role of cellular composition in the final
 627 objective, is to study a simplified version of the problem assuming cellular composition
 628 is at steady state (a common property of bacterial cells during exponential growth).
 629 We then propose a reduced version of the dynamical system by fixing the ribosomal
 630 concentration to a constant value r^* , which reduces the dimension of the model by
 631 one. Thus, the metabolite maximization problem is solved in terms of the parameter
 632 r^* , which represents a simpler analysis that can potentially provide an insight into
 633 the original optimization problem.

634 **5.1.1. Constant ribosomal concentration.** The system with Constant Ribo-
 635 somal Concentration r^* writes

$$636 \quad (\text{CRC-M}) \quad \begin{cases} \dot{s} = -w_M(s)(1 - r^*)\mathcal{V}, \\ \dot{p} = w_M(s)(1 - r^*) - \gamma w_R(p)(1 - r^*) - w_R(p)r^*(p + 1), \\ \dot{\mathcal{V}} = w_R(p)r^*\mathcal{V}. \end{cases}$$

637
 638 It can be seen that the study of the asymptotic behavior of system (S) applies to
 639 (CRC-M) as the latter is a particular case of the original one (S) with $r_0 = u^* = r^*$.
 640 We then maximize the final product x^* in terms of the constant ribosomal concentra-
 641 tion $r^* \in [r^-, r^+]$. The latter is given by the expression

$$642 \quad \max_{r^*} \lim_{t \rightarrow \infty} x(t).$$

643

We can see that the quantity

$$z = s + (p + 1)\mathcal{V} + \gamma \frac{1 - r^*}{r^*} \mathcal{V}$$

644 is constant. Thus,

$$645 \quad \mathcal{V}^* + \gamma \frac{1 - r^*}{r^*} (\mathcal{V}^* - \mathcal{V}_0) = \Sigma$$

646
647 which, using (3.3), yields

$$648 \quad x^* = \gamma \frac{1 - r^*}{r^*} (\mathcal{V}^* - \mathcal{V}_0).$$

650 Using the fact that $\mathcal{V}^* + x^* = \Sigma$ from (3.3), we see that x^* is monotone decreasing w.r.t.
651 r^* , and so the ribosomal concentration maximizing the infinite-time metabolite mass
652 is $r^* = r^-$. This is what one would expect intuitively in an infinite-time horizon, as
653 $r^* = r^-$ favors the production of metabolic proteins M, which catalyzes the synthesis
654 of metabolites X without arresting the production of biomass (given by the case
655 $r^* = 0$, which cannot be attained in trajectories starting in Γ). However, this kind
656 of strategies might perform sub-optimally for the finite horizon case, as not having
657 enough biomass can translate into a slow metabolite synthesis rate. Mathematically,
658 this is represented through the presence of \mathcal{V} in the dynamical equation of x . Similar
659 to previous results [27], a first phase dedicated to bacterial growth can also foster
660 the production of X, which depends directly on the concentration of bacteria in the
661 bioreactor.

662 5.2. Finite-time problem.

663 **5.2.1. Problem formulation.** In this section, we study the metabolite produc-
664 tion objective in (S) for a time interval $[0, t_f]$, in which the final concentration of
665 metabolite in the bioreactor $x(t_f)$ is maximized. While the biomass maximization
666 objective $\mathcal{V}(t_f)$ was already studied in model (WTB-M) (representing a wild-type
667 bacteria), it is likely that the presence of the heterologous pathway responsible for
668 the production of x might affect the results already obtained. Thus, the two objec-
669 tives are compared in model (S) from a numerical perspective. Given a fixed final
670 time $t_f > 0$, the OCP maximizing $c\mathcal{V}(t_f) + (1 - c)x(t_f)$ (with $c = \{0, 1\}$ depending
671 on the objective) with initial conditions (IC) writes

$$672 \quad \text{(MP-OCP)} \quad \left\{ \begin{array}{l} \text{maximize} \quad c\mathcal{V}(t_f) + (1 - c)x(t_f), \\ \text{subject to} \quad \text{dynamics of (S)}, \\ \quad \quad \quad \text{initial conditions (IC)}, \\ \text{and} \quad u(\cdot) \in \mathcal{U}, \end{array} \right.$$

673
674 It should be noted that the OCP is only valid for $c = 0$ (representing the metabolite
675 production objective) and $c = 1$ (for the biomass maximization objective), and thus
676 the intermediate values $c \in (0, 1)$ are not considered. One can easily see that, given
677 the dynamics of the system, applying PMP would yield a Hamiltonian linear in the
678 control for both values of c , which means that the solution of (MP-OCP) is similar to
679 that of (BM-OCP), given by expression (4.1). However, (MP-OCP) has an additional

680 level of complexity in comparison with (BM-OCP), produced by the presence of x in
 681 the model, as well as the term $-\gamma w_R(p)(1-r)$ in \dot{p} responsible for the consumption
 682 of resources for metabolite production. Thus, it was not possible to perform a study
 683 of the OCP using PMP. A numerical analysis of these results is provided in the next
 684 section.

685 **5.2.2. Numerical simulations.** The optimal trajectories were obtained follow-
 686 ing the same procedure as in the biomass maximization case. Figures 9, 10 and 11 are
 687 solutions of (MP-OCP) where the objective is the final-time product maximization
 688 $x(t_f)$ (obtained by fixing $c = 0$) for different final times t_f (40, 60 and 80, respec-
 689 tively) and with the same set of initial conditions. The metabolite synthesis rate is
 690 set to $\gamma = 0.5$. As expected, and similar to the results obtained for (BM-OCP), the
 691 optimal control takes the value $u = 0$ for most of the interval, representing an alloca-
 692 tion strategy that promotes the synthesis of proteins of the metabolic machinery M ,
 693 consequently catalyzing the absorption of nutrients from the medium and the produc-
 694 tion of x . Solutions are characterized by a short $u = 1$ bang arc at the beginning of
 695 the process, followed by a marginal singular arc before the final $u = 0$ bang arc. The
 696 latter suggests that a valid sub-optimal approximation of the optimal control could
 697 be a simple bang-bang (1-0) control law. In that case, the only degree of freedom
 698 would be the switching time between bang arcs, that can be easily computed through
 699 numerical optimization methods. Additionally, and as it can be seen across Figures 9,
 700 10 and 11, these results do not depend on the final time t_f : the final bang $u = 0$ of the
 701 optimal control is always predominant in the control strategy, and becomes larger as
 702 t_f increases. The finite-time numerical results are consistent with the results obtained
 703 for the infinite-time case in Section 5.1.1, in which the ribosomal sector of the cell r
 704 should be minimized to maximize the production of x . Figure 12 shows an optimal
 705 trajectory solution of (MP-OCP) with cost function $\mathcal{V}(t_f)$. In this case, the allocation
 706 strategy is described by an initial bang $u = 1$ followed by a singular arc that takes up
 707 most of the optimal solution, with values near to an intermediate strategy $u = 0.5$;
 708 and a short bang $u = 0$ at the end. Such strategy leads to a bacterial composition
 709 much more balanced between ribosomal and enzymatic proteins, in opposition to the
 710 metabolite production case (with $c = 0$ for (MP-OCP)), where most of the bacterial
 711 proteins were dedicated to the metabolic machinery. The latter behavior illustrates
 712 a natural trade-off between two opposed strategies: maximizing the number of ribo-
 713 somes to prioritize the synthesis of macromolecules over the production of x and, at
 714 the same time, maximizing the enzymatic activity in order to consume the substrate
 715 in the medium as fast as possible, towards (*Full depletion*).

716 Under the hypothesis that the mechanisms behind the allocation of cellular re-
 717 sources in bacteria have been optimized to outgrow competitors, it is coherent to
 718 think that a genetically modified bacteria (e.g. able to synthesize the metabolite
 719 X) would also maximize biomass. Thus, these internal mechanisms would produce
 720 a cellular composition profile similar to the one shown in Figure 12. Indeed, this is
 721 expected to happen even for artificially engineered specimens, as, in microorganisms,
 722 natural selection occurs very rapidly (even for time windows in the order of hours)
 723 due to the strong genetic variability of bacteria and their astonishingly high doubling
 724 rate. Then, interfering with this strategy so as to obtain allocations maximizing the
 725 production of metabolites in the bioreactor (as the ones shown in Figures 9, 10 and
 726 11) can be accomplished by externally shutting down the production of ribosomes at
 727 a certain time instant, which can be triggered by well-known biotechnological control
 728 techniques such as growth arrest [11].

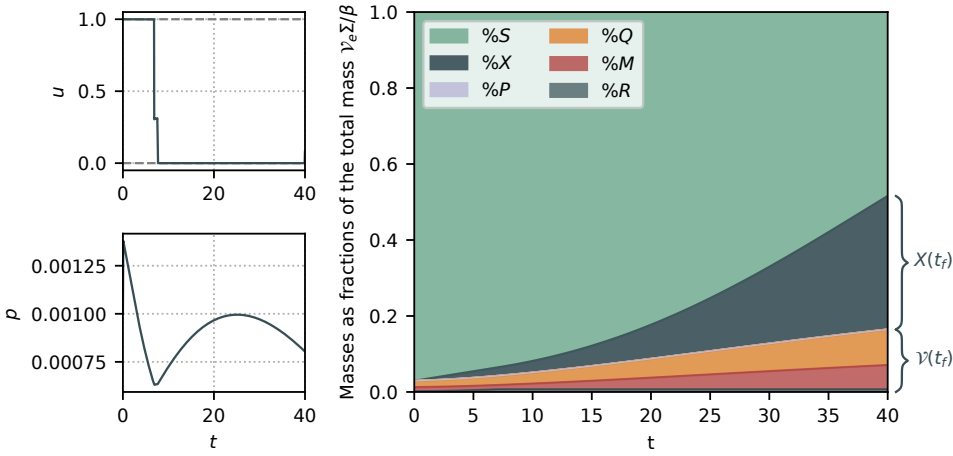


FIG. 9. Solution of (MP-OCP) for the metabolite maximization case $x(t_f)$, with $s_0 = 0.1$, $p_0 = 0.001$, $r_0 = 0.1$, $\mathcal{V}_0 = 0.003$ and $t_f = 60$. The final product concentration $x(t_f)$ is at 35% of the total mass in the bioreactor $\mathcal{V}_e \Sigma / \beta$, while the final volume $\mathcal{V}(t_f)$ is only at 16%.

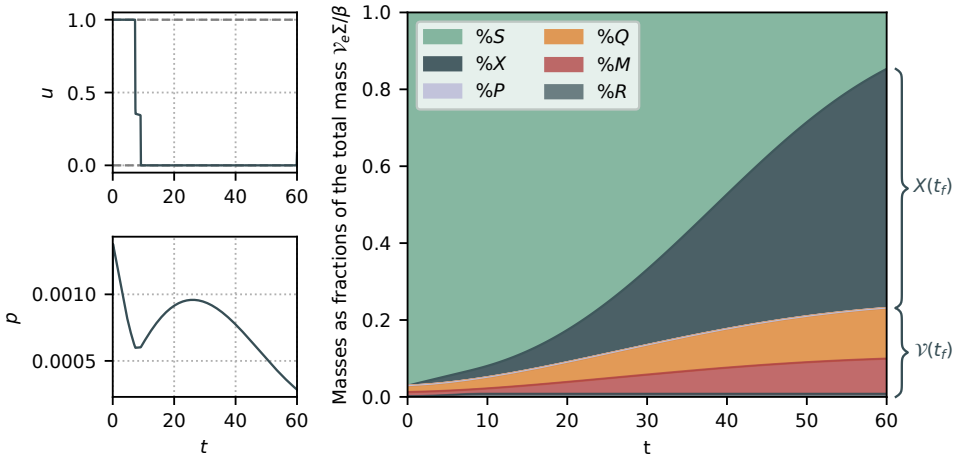


FIG. 10. Solution of (MP-OCP) for the metabolite maximization case $x(t_f)$, with $s_0 = 0.1$, $p_0 = 0.001$, $r_0 = 0.1$, $\mathcal{V}_0 = 0.003$ and $t_f = 60$. The final product concentration $x(t_f)$ is at 62% of the total mass in the bioreactor $\mathcal{V}_e \Sigma / \beta$, while the final volume $\mathcal{V}(t_f)$ is only at 23%.

729 **6. Discussion.** This paper presented a mathematical study of bacterial resource
 730 allocation in batch processing, and its applications to biomass and metabolite pro-
 731 duction. A dynamical model considering the production of a value-added chemical
 732 compound is proposed, and a study of the asymptotic behavior of the system based on
 733 mass conservation laws shows that, under all possible resource allocation strategies,
 734 all the substrate in the medium is consumed. Then, the particular case of a wild-type
 735 bacteria with no metabolite production is analyzed, showing that the optimal allo-
 736 cation propitious for biomass maximization—and thus, competitors outgrowing—is
 737 accomplished through a rather low value of the optimal control u , which yields a very
 738 high m/r ratio (i.e. the ratio of enzymatic to ribosomal mass fractions) in the cell

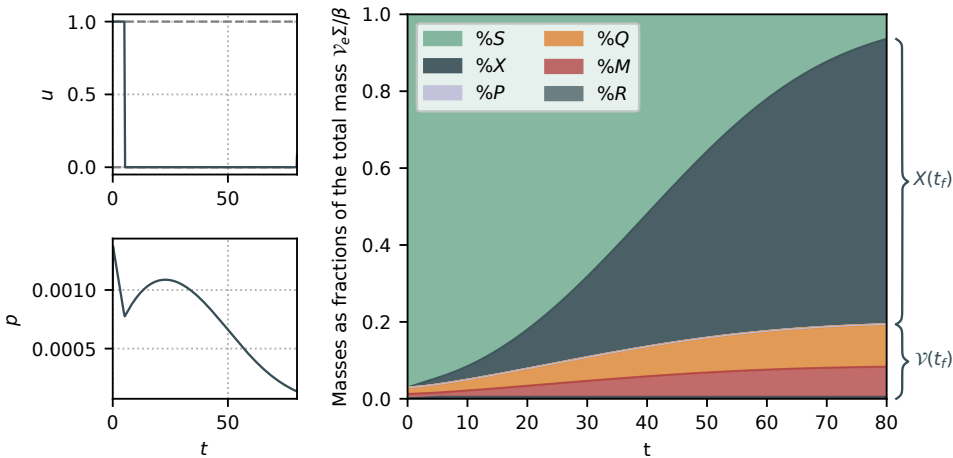


FIG. 11. *Solution of (MP-OCP) for the metabolite maximization case $x(t_f)$, with $s_0 = 0.1$, $p_0 = 0.001$, $r_0 = 0.1$, $\mathcal{V}_0 = 0.003$ and $t_f = 60$. The final product concentration $x(t_f)$ is at 74% of the total mass in the bioreactor $\mathcal{V}_e \Sigma / \beta$, while the final volume $\mathcal{V}(t_f)$ is only at 19%.*

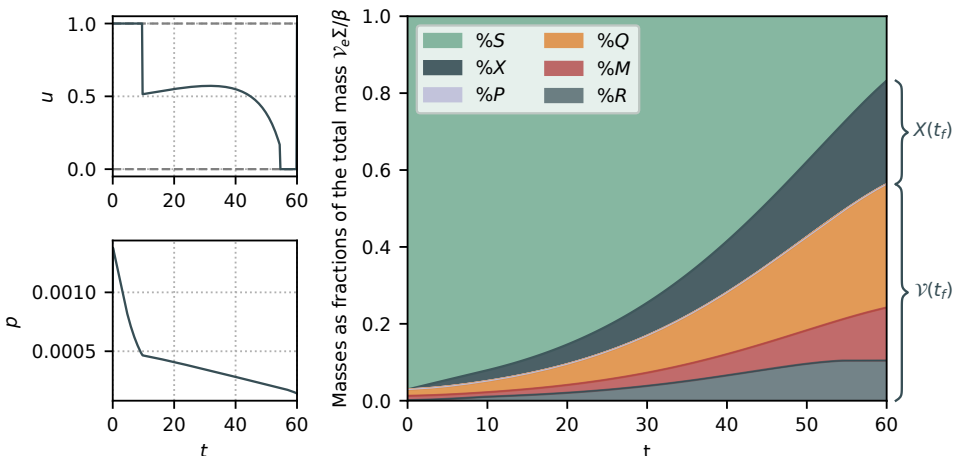


FIG. 12. *Solution of (MP-OCP) for the biomass maximization case $\mathcal{V}(t_f)$, with $s_0 = 0.1$, $p_0 = 0.001$, $r_0 = 0.1$, $\mathcal{V}_0 = 0.003$ and $t_f = 60$. The final product concentration $x(t_f)$ is at 27% of the total mass in the bioreactor $\mathcal{V}_e \Sigma / \beta$, while the final volume $\mathcal{V}(t_f)$ is at 56%.*

739 throughout the bioprocess. Paradoxically, for the metabolite production case, this
 740 kind of strategies would rather maximize the production of x , while for maximizing
 741 the biomass under the presence of the heterologous pathway, a more balanced cel-
 742 lular composition is required. Overall, results show that optimal allocation can be
 743 accomplished through a two-phase control: a first phase of pure bacterial growth ded-
 744 icated to produce as many ribosomal proteins as possible; followed by a production
 745 phase where the remainder of the feedstock is used to synthesize the compound of
 746 interest. While the first phase matches the natural bacterial behavior, the second
 747 one requires human intervention to arrest the production of ribosomes (by externally

748 setting $u = 0$). The obtained two-phased external control profile is in close agreement
749 with well-known metabolic engineering techniques used in microbial cell factory [27].

750 The analysis presented in this paper raises interesting questions both from math-
751 ematical and biological points of view. For instance, it would be worthwhile to further
752 study the potential presence (or absence) of the turnpike phenomenon in the optimal
753 control solutions. Depending on the complexity of the OCP, it is often possible to
754 obtain an analytical proof of the exponential convergence of the singular arc to the
755 solution of the static OCP [25], and to find an explicit link between the length of the
756 singular arc and the duration of the bioprocess. From a biological perspective, includ-
757 ing additional substrates could broaden the approach to represent other well-studied
758 phenomena observed in bacterial growth. For example, under the presence of differ-
759 ent nutrients in the culture, bacteria tend to favor (i.e. consume first) those that are
760 easier to metabolize, which is a phenomenon known as diauxic growth. This behavior
761 has been extensively studied from an optimal control viewpoint, but without taking
762 into consideration cellular composition. Formulating more comprehensive dynamical
763 models and studying their associated OCPs can be instrumental in understanding
764 natural allocation strategies in microbial growth, and in engineering synthetic control
765 schemes targeting industrial objectives.

766 **Acknowledgments.** The authors thank Hidde de Jong (Microcosme team, Inria
767 Grenoble – Rhône-Alpes) for many discussions on the biological context. We also
768 appreciate the help of Sacha Psalmon and Baptiste Schall, from Polytech Nice Sophia,
769 for the numerical simulations and the production of the online example in the control
770 toolbox gallery.⁵

771

REFERENCES

- 772 [1] A. A. AGRACHEV AND Y. SACHKOV, *Control Theory from the Geometric Viewpoint*, vol. 87,
773 Springer Science & Business Media, 2013.
- 774 [2] M. BASAN, M. ZHU, X. DAI, M. WARREN, D. SÉVIN, Y.-P. WANG, AND T. HWA, *Inflating*
775 *bacterial cells by increased protein synthesis*, *Molecular systems biology*, 11 (2015), p. 836.
- 776 [3] V. BORISOV, *Fuller's phenomenon*, *Journal of Mathematical Sciences*, 100 (2000), pp. 2311–
777 2354.
- 778 [4] J.-B. CAILLAU, W. DJEMA, J.-L. GOUZÉ, S. MASLOVSKAYA, AND J.-B. POMET, *Turnpike prop-*
779 *erty in optimal microbial metabolite production*, *J. Optim. Theory. Appl.*, 194 (2022),
780 pp. 375–407.
- 781 [5] E. CINQUEMANI, F. MAIRET, I. YEGOROV, H. DE JONG, AND J.-L. GOUZÉ, *Optimal control of*
782 *bacterial growth for metabolite production: The role of timing and costs of control*, in 2019
783 18th European Control Conference (ECC), IEEE, 2019, pp. 2657–2662.
- 784 [6] H. DE JONG, J. GEISELMANN, AND D. ROPERS, *Resource reallocation in bacteria by reengineering*
785 *the gene expression machinery*, *Trends in microbiology*, 25 (2017), pp. 480–493.
- 786 [7] N. GIORDANO, F. MAIRET, J.-L. GOUZÉ, J. GEISELMANN, AND H. DE JONG, *Dynamical allo-*
787 *cation of cellular resources as an optimal control problem: novel insights into microbial*
788 *growth strategies*, *PLoS computational biology*, 12 (2016), p. e1004802.
- 789 [8] R. HEINRICH AND S. SCHUSTER, *The regulation of cellular systems*, Springer Science & Business
790 Media, 2012.
- 791 [9] S. HUI, J. M. SILVERMAN, S. S. CHEN, D. W. ERICKSON, M. BASAN, J. WANG, T. HWA,
792 AND J. R. WILLIAMSON, *Quantitative proteomic analysis reveals a simple strategy of global*
793 *resource allocation in bacteria*, *Molecular systems biology*, 11 (2015), p. 784.
- 794 [10] L. HUO, J. J. HUG, C. FU, X. BIAN, Y. ZHANG, AND R. MÜLLER, *Heterologous expression*
795 *of bacterial natural product biosynthetic pathways*, *Natural Product Reports*, 36 (2019),
796 pp. 1412–1436.

⁵ct.gitlabpages.inria.fr/gallery/substrate/depletion.html

- 797 [11] J. IZARD, C. D. G. BALDERAS, D. ROPERS, S. LACOUR, X. SONG, Y. YANG, A. B. LINDNER,
798 J. GEISELMANN, AND H. DE JONG, *A synthetic growth switch based on controlled expression*
799 *of RNA polymerase*, *Molecular systems biology*, 11 (2015), p. 840.
- 800 [12] G. JEANNE, A. GOELZER, S. TEBBANI, D. DUMUR, AND V. FROMION, *Dynamical resource*
801 *allocation models for bioreactor optimization*, *IFAC-PapersOnLine*, 51 (2018), pp. 20–23.
- 802 [13] F. MAIRET, J.-L. GOUZÉ, AND H. DE JONG, *Optimal proteome allocation and the temperature*
803 *dependence of microbial growth laws*, *NPJ systems biology and applications*, 7 (2021),
804 pp. 1–11.
- 805 [14] D. MOLENAAR, R. VAN BERLO, D. DE RIDDER, AND B. TEUSINK, *Shifts in growth strategies*
806 *reflect tradeoffs in cellular economics*, *Molecular systems biology*, 5 (2009), p. 323.
- 807 [15] L. S. PONTRYAGIN, *Mathematical theory of optimal processes*, Routledge, 2018.
- 808 [16] M. SCOTT, C. W. GUNDERSON, E. M. MATEESCU, Z. ZHANG, AND T. HWA, *Interdependence of*
809 *cell growth and gene expression: origins and consequences*, *Science*, 330 (2010), pp. 1099–
810 1102.
- 811 [17] M. SCOTT, S. KLUMPP, E. MATEESCU, AND T. HWA, *Emergence of robust growth laws from*
812 *optimal regulation of ribosome synthesis*, *Molecular Systems Biology*, 10 (2014), p. 747.
- 813 [18] I. S. TEAM COMMANDS, *Bocop: an open source toolbox for optimal control*. <http://bocop.org>,
814 2017.
- 815 [19] E. TRÉLAT AND E. ZUAZUA, *The turnpike property in finite-dimensional nonlinear optimal*
816 *control*, *Journal of Differential Equations*, 258 (2015), pp. 81–114.
- 817 [20] A. Y. WEISSE, D. A. OYARZÚN, V. DANOS, AND P. S. SWAIN, *Mechanistic links between cellular*
818 *trade-offs, gene expression, and growth*, *Proceedings of the National Academy of Sciences*,
819 112 (2015), pp. E1038–E1047.
- 820 [21] A. G. YABO, *Optimal resource allocation in bacterial growth: theoretical study and applications*
821 *to metabolite production*, PhD thesis, Université Côte d’Azur, 2021, [https://theses.hal.](https://theses.hal.science/tel-03636842)
822 [science/tel-03636842](https://theses.hal.science/tel-03636842).
- 823 [22] A. G. YABO, J.-B. CAILLAU, AND J.-L. GOUZÉ, *Singular regimes for the maximization of*
824 *metabolite production*, in 2019 IEEE 58th Conference on Decision and Control (CDC),
825 IEEE, 2019, pp. 31–36.
- 826 [23] A. G. YABO, J.-B. CAILLAU, AND J.-L. GOUZÉ, *Optimal bacterial resource allocation: metab-*
827 *olite production in continuous bioreactors*, *Mathematical Biosciences and Engineering*, 17
828 (2020), pp. 7074–7100.
- 829 [24] A. G. YABO, J.-B. CAILLAU, AND J.-L. GOUZÉ, *Optimal allocation of bacterial resources in fed-*
830 *batch reactors*, in 2022 European Control Conference (ECC), IEEE, 2022, pp. 1466–1471.
- 831 [25] A. G. YABO, J.-B. CAILLAU, J.-L. GOUZÉ, H. DE JONG, AND F. MAIRET, *Dynamical analysis*
832 *and optimization of a generalized resource allocation model of microbial growth*, *SIAM*
833 *Journal on Applied Dynamical Systems*, 21 (2022), pp. 137–165.
- 834 [26] A. G. YABO AND J.-L. GOUZÉ, *Optimizing bacterial resource allocation: metabolite production*
835 *in continuous bioreactors*, *IFAC-PapersOnLine*, 53 (2020), pp. 16753–16758.
- 836 [27] I. YEGOROV, F. MAIRET, H. DE JONG, AND J.-L. GOUZÉ, *Optimal control of bacterial growth*
837 *for the maximization of metabolite production*, *Journal of mathematical biology*, 78 (2019),
838 pp. 985–1032.